AD-A235 979

REPORT DOCUMENTATION PAGE

Form Approved
OMB No. 0704-0188

1. AGENCY USE ONLY (Leave blank)

2. REPORT DATE: 15 May 1991

3. REPORT TYPE AND DATES COVERED: Reprint

4. TITLE AND SUBTITLE: Average Height-Integrated Joule Heating Rates and Magnetic Deflection Vectors due to Field-Aligned Currents During Sunspot Minimum

5. FUNDING NUMBERS: PE 61102F, PR 2311, TA G5, WU 02

6. AUTHOR(S): F.J. Rich, M.S. Gussenhoven, D.A. Hardy, E. Holeman*

7. PERFORMING ORGANIZATION NAME(S) AND ADDRESS(ES): Phillips Laboratory (PHG), Hanscom AFB, MA 01731-5000

8. PERFORMING ORGANIZATION REPORT NUMBER: PL-TR-91-2118

9. SPONSORING/MONITORING AGENCY NAME(S) AND ADDRESS(ES)

10. SPONSORING/MONITORING AGENCY REPORT NUMBER

11. SUPPLEMENTARY NOTES: * Physics Department, Boston College, Chestnut Hill, MA 02167 - Reprinted from Journal of Atmospheric and Terrestrial Physics, Vol. 53, No. 3/4 pp 293-308,1991

12a. DISTRIBUTION/AVAILABILITY STATEMENT: Approved for public release; Distribution unlimited

12b. DISTRIBUTION CODE

13. ABSTRACT (Maximum 200 words)

Abstract—Height-integrated Joule heating has been calculated from simultaneous observations of field-aligned currents and precipitating electrons made by the Defense Meterorological Satellite Program (DMSP) satellite F7. The DMSP/F7 satellite provided nearly continuous data from January 1984 to October 1987. In this paper we use data from January 1984 to December 1985, a period of nearly uniform, low solar EUV flux near the minimum of the sunspot cycle. By assuming that the majority of the observed field-aligned currents connect through the ionosphere via local Pedersen currents, we have calculated the local Joule heating rates. By combining Joule heating observations from multiple orbits, a survey of Joule heating vs magnetic latitude, magnetic local time, magnetic activity level and season has been compiled. In addition, the average magnetic deflection vector has been compiled. Our survey of the distribution of Joule heating has finer resolution than previous surveys, and is comparable with previous case studies. We have found evidence that the source of the field-aligned current into/out of the dayside cusp is on open field lines and that the source of the field-aligned current into/out of the auroral zones is on closed field lines.

14. SUBJECT TERMS: Ionosphere, Joule heating, DMSP, Aurora

15. NUMBER OF PAGES: 16

16. PRICE CODE

17. SECURITY CLASSIFICATION OF REPORT	18. SECURITY CLASSIFICATION OF THIS PAGE	19. SECURITY CLASSIFICATION OF ABSTRACT	20. LIMITATION OF ABSTRACT
UNCLASSIFIED	UNCLASSIFIED	SAR	SAR

Journal of Atmospheric and Terrestrial Physics, Vol. 53, No. 3/4, pp. 293–308, 1991.
Printed in Great Britain.
0021-9169/91 $3.00 + .00
Pergamon Press plc

Average height-integrated Joule heating rates and magnetic deflection vectors due to field-aligned currents during sunspot minimum

F. J. RICH,* M. S. GUSSENHOVEN,* D. A. HARDY* and E. HOLEMAN†

*Space Physics Division, Geophysics Laboratory (AFSC), Hanscom Air Force Base, Bedford, MA 01731, U.S.A.; †Physics Department, Boston College, Chestnut Hill, MA 02167, U.S.A.

(Received in final form 30 August 1990)

Abstract—Height-integrated Joule heating has been calculated from simultaneous observations of field-aligned currents and precipitating electrons made by the Defense Meterorological Satellite Program (DMSP) satellite F7. The DMSP/F7 satellite provided nearly continuous data from January 1984 to October 1987. In this paper we use data from January 1984 to December 1985, a period of nearly uniform, low solar EUV flux near the minimum of the sunspot cycle. By assuming that the majority of the observed field-aligned currents connect through the ionosphere via local Pedersen currents, we have calculated the local Joule heating rates. By combining Joule heating observations from multiple orbits, a survey of Joule heating vs magnetic latitude, magnetic local time, magnetic activity level and season has been compiled. In addition, the average magnetic deflection vector has been compiled. Our survey of the distribution of Joule heating has finer resolution than previous surveys, and is comparable with previous case studies. We have found evidence that the source of the field-aligned current into/out of the dayside cusp is on open field lines and that the source of the field-aligned current into/out of the auroral zones is on closed field lines.

1. INTRODUCTION

The input of energy to the ionosphere is important to the dynamics and structure of the upper atmosphere. Energy deposited in the ionospheric E-layer and lower F-layer is transferred to the neutral atmosphere, or 'thermosphere' at altitudes of 90–300 km. The result of this energy deposition is a change in the neutral density at altitudes of 90–600 km which affects the drag on low-altitude satellites and changes their position and orbit lifetime. At magnetic latitudes below 55°, solar UV which varies with the 11 yr sunspot cycle is the dominant source of energy input to the ionosphere and neutral atmosphere. At high latitudes, the five major sources of energy input in their approximate order of importance are: solar UV, Joule heat, precipitation of energetic (5 eV–30 keV) particles (especially electrons), plasma wave heating and energy transport from the lower atmosphere. In winter when the solar UV input is low or absent, Joule heating, particle precipitation and energy transport from the lower atmosphere are the dominant energy inputs to the high-latitude atmosphere in the altitude range of 90–600 km.

Joule heating is the transfer of momentum from ionospheric ions to the neutrals. The ions gain momentum from an electric field imposed upon the high-latitude ionosphere by the magnetosphere. The electric field, and thus the ion momentum, increases in strength and affects a wide area as geomagnetic activity increases. In most cases, most of the momentum transfer occurs in the ionospheric E-layer (90–160 km altitude). The transferred momentum partially goes into a temperature increase of the thermosphere and ionosphere and partially into a change in the neutral wind velocity. BUCHERT and LA HOZ (1988) reported a highly local, highly disturbed case when $v_{ions} \approx 3.8$ km/s (or equivalently $E \approx 190$ mV/m), which transferred energy to the ions and neutrals causing $T_{ions} \approx 12{,}000$K and $v_{neutral} \approx 600$ m/s in the F-region. If the ionospheric electric field is roughly constant for several hours, both the E-region and F-region neutral winds will be deviated toward the same direction as the ion convection. In the lower F-region, the neutral winds can almost be the same as the ion flow velocity. The E-region neutral winds are deviated by a few hundred meters per second or less. As the neutral flow is deviated toward the ion flow, the ion flow momentum transfer decreases.

The energy input to the high-latitude ionosphere from particle precipitation has been extensively surveyed using data from the DMSP satellites, using data from the NOAA/TIROS satellites (FULLER-ROWELL and EVANS, 1987) and by other researchers. HARDY et al. (1985, 1989) and GUSSENHOVEN et al. (1985) have given detailed maps of the energy flux of precipitating electrons and ions observed by DMSP. HARDY et al. (1987) have calculated average height-integrated

conductivities due to precipitating electrons observed by DMSP. The energy input from Joule heating has not been as extensively studied because it cannot be measured as easily or as directly. Studies have shown that Joule heat represents 60–90% of the energy input from the magnetosphere to the ionosphere [e.g. VICKREY *et al.* (1982), EMERY *et al.* (1985), EVANS *et al.* (1987) and AHN *et al.* (1989a)].

While the solar UV input is slowly varying, the energy input from Joule heating and precipitating particles varies over several orders of magnitude (from >0.1 W/m^2 to <0.001 W/m^2 in local areas and from $>10^{11}$ W to $<10^9$ W across the high-latitude region) on time scales of geomagnetic storms and substorms. Geomagnetic substorms generally occur several times per day with a rise time of 10–20 min and decay time of 30 min–2 h. Geomagnetic storms occur 10–20 times per year with a rise time of 1–12 h and a decay time of 1–6 days. Geomagnetic substorms occur more frequently and with more intensity during storm periods.

During geomagnetically active periods, the density of the neutrals in the altitude range from 90 to 600 km during the winter season changes by 50–200% relative to geomagnetically quiet periods. The MSIS model (HEDIN *et al.*, 1977a, b; HEDIN, 1983, 1987) is a statistical computer model widely used to calculate the neutral density profile of the thermosphere. The MSIS model is a complex table-look-up algorithm based upon the average observations obtained under varying conditions. The MSIS model has a simple method of varying the neutral density with geomagnetic activity which is dependent on the instantaneous geomagnetic activity, weakly dependent on the history of geomagnetic activity, weakly dependent on magnetic latitude and independent of magnetic local time. By comparing the density observed with satellites in the altitude range of 300–600 km, MARCOS (1989) found the standard deviation between the measured and model values to be approximately 5% near the Equator for all levels of geomagnetic activity and 15–20% at high latitude during active periods, with individual observations differing by more than 30%. A physical computer model of the neutrals at high latitude is the Thermospheric General Circulation Model (TGCM) (KILLEEN and ROBLE, 1984, 1986). The TGCM computer model includes a set of fluid dynamic expressions to follow a model thermosphere with time varying heat inputs. The TGCM model can account for phenomena such as the time delay between the input of heat to the ionosphere and the increase of drag for low-altitude satellites. In principle, a physical model can provide a more accurate description of the thermosphere than a statistical model if the inputs to the physical model are complete and accurate enough. However, the TGCM or a similar dynamic model needs many inputs. One of these is an accurate time series describing the latitudinal and local time distribution and the quantity of Joule heat flowing into the high-latitude ionosphere.

Height-integrated Joule heating (W/m^2) of the high-latitude ionosphere can be determined by several different techniques. KILLEEN *et al.* (1984) used simultaneous measurements of the ionospheric plasma drift velocity and the neutral wind velocity to determine the differential velocity which is used together with a model atmosphere to determine the Joule heating rates. BARON and WAND (1983) used incoherent radar to measure ion drifts, which cause Joule heating, and the ion and neutral temperature enhancements, which are caused by Joule heating. KAMIDE and BAUMJOHANN (1985) and KAMIDE *et al.* (1989) have used data from a network of ground magnetometers to determine the horizontal ionospheric currents which are used together with a model of ionospheric conductivity to determine the Joule heating rates. KAMIDE *et al.* (1986) and AHN *et al.* (1989a, b) used ground magnetometer data to determine ionospheric currents and satellite data to determine ionospheric conductivity to calculate Joule heating for individual timeperiods. AHN *et al.* (1989b) also showed that the use of model conductivities instead of conductivities obtained simultaneously with the currents can significantly affect the Joule heat calculations. HEELIS and COLEY (1988) used ion drift data with ion temperature data from DE-2 to obtain the local Joule heating rate (W/m^3) and the ion drifts with a model conductivity to obtain the height-integrated Joule heating rate. FOSTER *et al.* (1983) and RICH *et al.* (1987) used simultaneous satellite data to estimate both the current and the conductivity.

For this study we use simultaneous magnetic field and precipitating electron data from a low-altitude, polar-orbiting satellite to calculate the Joule heat per unit area along the satellite track. By using a large body of data from many satellite passes through the high-latitude region, we have determined the average Joule heat input as a function of magnetic latitude, magnetic local time, geomagnetic activity, season and orientation of the Interplanetary Magnetic Field (IMF). The basic method of calculating the Joule heat along the satellite track was given by RICH *et al.* (1987) using the DMSP/F7 satellite as the source of the data. For this study, we have modified the method as described below. We have used 2 yr of DMSO/F7 data consisting of approximately 6000 orbits (12,000 passes). Here we report on the results of the survey.

2. INSTRUMENTATION

Magnetic field and particle precipitation measurements are taken from the DMSP/F7 satellite, which was placed into a circular, polar orbit at 832 km altitude in November 1983. Data are available almost continuously from December 1983 to October 1987. In this study, we used all available data from 1 January 1984 to 31 December 1985. The solar cycle was near the minimum during this period; the monthly average of the 10.7-cm radio flux, which is assumed to correlate well with the solar EUV flux and the sunspot number, was always close to 80×10^{-22} W/(m^2 Hz), adjusted to 1 AU. Thus the results of this report are representative only of sunspot minimum conditions.

The satellite orbit plane is Sun-synchronous along the 1030–2230 Local Time meridian and has a 98.7° inclination. Due to the offset of the geomagnetic pole from the geographic pole, the satellite crosses most magnetic latitude/magnetic local time regions poleward of 55° after combining the northern and southern hemisphere orbit tracks. The only high-latitude region not observed lies approximately from 2 to 6 h magnetic local time and from 55 to 70°. The portions of the high-latitude regions covered are illustrated in Fig. 1. Data for the areas not observed have been estimated by interpolation of values from earlier and later local times on the same magnetic latitude.

The satellite attitude is fixed in a local vertical coordinate system. The DMSP coordinate system is used herein. It consists of (x, y, z) = (down, forward, cross-track). The direction of travel makes this coordinate system approximately a local vertical system of (down, north/south, east/west), especially when the orbit track passes very close to the magnetic pole. Since the auroral oval is well approximated by a circle centred slightly to the night side of the magnetic pole, the y-axis is generally perpendicular to the oval and to the plane of large-scale, field-aligned current sheets and the z-axis is generally parallel to the current sheets.

The magnetometer instrument (which is given the acronym 'SSM') is body-mounted and obtains 20 vector samples per second with a resolution of 12.2 nT per axis. The magnetometer measures magnetic fields from both geophysical and local spacecraft sources. By use of a geomagnetic field model and data filters, all signatures except those from the field-aligned currents are removed from the data. The particle spectrometer (acronym 'SSJ/4') measures one ion and one electron spectrum each second, in 20 channels, logarithmically spaced in energy from 30 eV to 30 keV. The particle spectrometer has a fixed aperture looking vertically upward. Further description of the instruments is given by RICH *et al.* (1985).

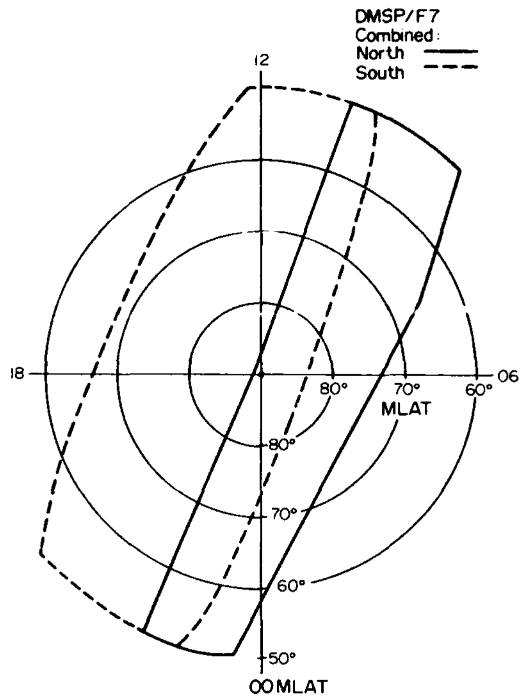

Fig. 1. Portions of the northern and southern high-latitude regions in geomagnetic coordinates, which are observed by DMSP/F7, are shown with the solid and dotted lines, respectively.

3. DATA

3.1. *Method of calculation*

The theory for our Joule calculations was given by RICH *et al.* (1987). We calculate the height-integrated Joule heating rate for the portion of the E-layer on the same field line as the satellite by calculating the height-integrated conductivities and ionospheric currents from DMSP data. The total conductivity is obtained from the conductivity created by measured precipitating electrons and from a model of the conductivity created by EUV radiation. The ionospheric currents are obtained from the simultaneously measured field-aligned currents and an assumption that the majority of field-aligned currents are locally connected by Pedersen currents. The method we use is independent of the neutral winds; the actual currents flowing into and out of the ionosphere yield the effective electric field driving the currents (the electric field in the rest frame of the ionospheric plasma) instead of yielding the magnetospheric electric field.

If all background levels are removed from the magnetic field data, then the magnitude of the field-aligned currents, and in turn the Pedersen currents, should

be proportional to the magnitude of the magnetic deflection vector. Unfortunately, removal of the geomagnetic field using standard models leaves a residual of a few hundred nT, which varies slowly along the satellite path. The residual is significantly larger in the southern hemisphere than in the northern hemisphere due to the difference of geomagnetic survey data in the two hemispheres, especially near the poles. Also, the removal of the spacecraft magnetic field leaves a random residual of a few tens of nT. A low-pass Fourier transform was considered and discarded because it removed trends within regions of activity as well as trends due to errors in the model geomagnetic field. Instead, we fit the latitudinal variation of the magnetic deflection vector outside regions of auroral precipitation and field-aligned currents to a polynomial. The polynomial was then used to interpolate a baseline through the region of field-aligned currents. This baseline was then subtracted from all data in the high-latitude portion of the orbit to obtain the residual ΔBs.

The procedure for finding the polynomial is as follows: firstly, we calculate the average and root-mean-square (r.m.s.) for each 30 s section of magnetic field data. If the r.m.s. for a 30 s period is less than 20 nT for ΔB_y and 30 nT for ΔB_z, and if the geomagnetic latitude is within an acceptable range, then the average values are used to calculate the polynomial functions for $\Delta B_y(t)$ and $\Delta B_z(t)$ for a polar pass. The definition of an acceptable latitude range is an addition to the method used by Rich et al. (1987). The acceptable latitude range is from 11.0 to 2.0° equatorward of the average equatorward boundary for ion precipitation, and from 9.0° poleward of this boundary to the highest latitude reached by the satellite if the highest latitude reached is greater than 9.0° poleward of the ion precipitation boundary. If the satellite's highest latitude for a pass is less than 9.0° poleward of the ion precipitation boundary, then acceptable latitudes are all of those poleward of 11.0° equatorward of the ion precipitation boundary. The equatorward boundary of the ion precipitation is estimated for a given pass by using the average maps of ion precipitation produced by Hardy et al. (1989) and the K_p level during the pass. For regions longer than 120 s which do not meet these criteria, artificial average values are created approximately every 60 s by a linear interpolation of acceptable values on either side of the gap. This keeps the polynomial functions well behaved within a gap. The polynomial functions are calculated by a least-squares fit of the average values to an odd-ordered polynomial of order 9 or less. The polynomial functions are then subtracted from all the ΔB_y or ΔB_z values in a high-latitude pass. A significant problem with the use of the polynomial technique is that geophysically real deflections at very high latitudes in the polar cap are removed. Standard low-pass filtering techniques would have the same effect. After removing the polynomial, the spacecraft 'noise' is eliminated by reducing the magnitude of all values of ΔB_y or ΔB_z by 50 nT. For very low levels of activity, this causes an underestimate of the Joule heating, but since Joule heat is proportional to the square of the magnetic deflections, the Joule heat during moderate to high auroral activity ($\Delta B > 300$ nT) is negligibly affected.

In Fig. 2, we show an example of the application of this technique. We note that the magnetic deflection outside the region of auroral field-aligned currents is clearly not zero and cannot be fitted by a straight line, especially the ΔB_y component. The deviation of the baseline from zero or a straight line for the data shown in Fig. 2 is worse than most cases. In general, the deviation is greater in the southern high-latitude region than in the northern region. The baseline for the ΔB_z component in Fig. 2 might be slightly closer to a straight line than the polynomial fit if there is a small, but real negative deflection in the polar cap region (943–949). We have chosen to define the deflections in the polar cap as zero instead of devising a method of estimating the small deflection vectors there. This bias in our method has little effect on the global pattern of Joule heat since it is small in the polar regions, but this bias does affect the average ΔB in the polar cap and will affect future efforts to calculate field-aligned currents from the maps of average ΔB.

After correcting for the residual deflections in the magnetic field data, the Joule heat at each second along the high-latitude portion is calculated, and both the Joule heat and the magnetic deflection vectors are stored in a data base. Before the magnetic deflection vectors are stored, they are rotated from a spacecraft coordinate system to a geomagnetic, local vertical system. In that system, one axis lies in the horizontal plane and points toward the corrected geomagnetic north, and the other axis points toward corrected geomagnetic east. This introduces a small error at high latitude because this coordinate system carries the assumption that the geomagnetic field vector is radial. However, since the x-axis (vertical axis) of the magnetometer data has more spacecraft 'noise' than the horizontal axes, we are introducing a small error in order to avoid a larger error. To match the magnetic deflection vectors in the southern hemisphere with those in the northern hemisphere, we rotate the deflection vectors in the southern hemisphere by 180 before placing them in the data base.

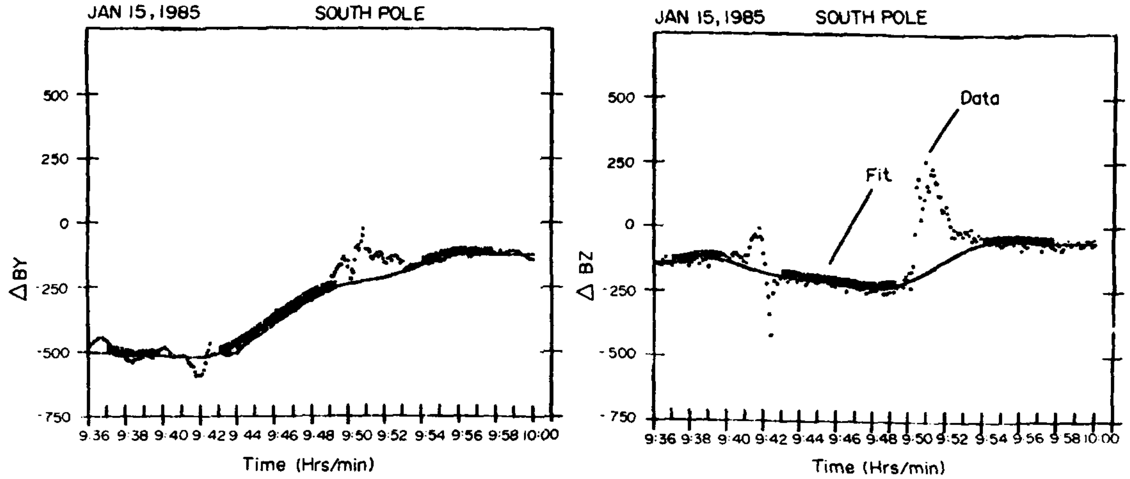

Fig. 2. An example of the use of a polynomial to fit the very low frequency variations in the magnetic deflections outside of regions of auroral activity. Both the data and polynomial are plotted. For the polynomial, large symbols are plotted in regions where the polynomial was fitted to the magnetic data and small symbols in regions where the data were not fitted. The bottom of the large symbols marks the value of the polynomial being plotted. All data are plotted with small symbols. The data were obtained in the southern high-latitude region during a period when the geomagnetic activity index K_p was 2 (moderately low activity).

The data base for the Joule heat and deflection vectors is sorted into 35 bins for magnetic latitude from 55 to the pole, by 48 bins in magnetic local time, by 2 bins for the north and south high-latitude regions, by 4 bins for seasons, by 2 bins for Interplanetary Magnetic Field (IMF) toward and away sectors, and by 7 bins of geomagnetic activity based upon the 3-h K_p index. The IMF toward (IMF $B_x > 0$) and away (IMF $B_x < 0$) structures are determined from a 'voting scheme' using solar observations, IMF measurements and ground magnetometers. The results are shown in Fig. 3. On average, toward and away sectors correspond to IMF $B_y < 0$ and $B_y > 0$, respectively. During days when the Earth is passing through a boundary in the IMF sector structure, the F7 data are excluded from the data base. During days when the IMF B_x component changes sign for a portion of a day due to a passing disturbance in the solar wind, the data are retained in the bin for the IMF sector within which the disturbance is embedded. A restriction to using only the IMP 8 data to specify the sectors instead of all three data sets would have vastly decreased the usable data, resulting in fewer bins with statistically meaningful results. The K_p bins are 0 to 0+, 1− to 1+, ..., 5− to 5+ and 6− to 9. The three seasons are chosen as equinox, winter solstice and summer solstice ±45 days.

The results we present here were produced by combining and averaging data from appropriate bins. In cases in which there might be a systematic difference between bins, we examined the bins separately before combining them. For example, we started by sorting data separately for northern hemisphere spring and fall for each IMF sector and for southern hemisphere spring and fall. We found no systematic variation in the North Pole spring and fall data for away sectors when compared with South Pole spring and fall data in toward sectors. Similarly, comparing North Pole summer months (May, June, July) for away sectors with South Pole summer months (November, December, January) for toward sectors, we found no systematic variations. We show here only equinox, summer and winter data associated with the appropriate IMF sector. The annotation in the figures such as 'North Toward+South Away' is an abbreviation for a combination of northern hemisphere data during toward sectors of the IMF with southern hemisphere data during away sectors.

3.2. *Smoothing algorithm*

A final step in our data handling is to smooth the value in the bins to remove random variations in adjoining bins due to a finite sample size and residual

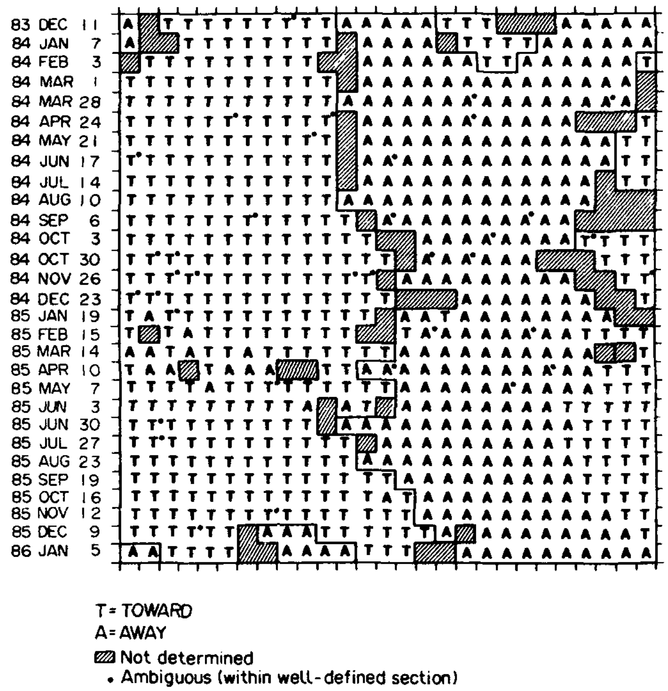

Fig. 3. Interplanetary Magnetic Field (IMF) sectors determined from an analysis of ground magnetometer data in the polar caps and of polar rain data for the period used in this report.

noise. The smoothing is done by applying the following algorithm:

$$V'_{i,j} = [4*V_{i,j}+V_{i-1,j}+V_{i+1,j}+V_{i,j-1}+V_{i,j+1}]/8.$$

If one of the neighboring points does not exist, then it is dropped from the above expression and the divisor is reduced by 1. For a second level of smoothing, the algorithm is applied again on the results of the first smoothing, and so forth for higher levels of smoothing. The disadvantage of smoothing is that it spreads out the area having non-zero values and decreases the magnitude of all values. We have found that applying the algorithm three times provides a good balance between the advantages and disadvantages of smoothing. As mentioned above, bins without data are filled by interpolating from data in bins on the same magnetic latitude.

4. RESULTS

4.1. *Average height-intergrated Joule heating*

In Figs 4–6, we show typical contour plots of the height-integrated Joule heating as a function of geomagnetic latitude and local time as determined in this study. The region of significant Joule heating is shaped like a ring and approximately overlays the auroral oval. There are maxima in the Joule heating rate near the expected extrema in the high-latitude electrostatic potential pattern (near 04 and 15 h magnetic local time in the auroral zone) and near the dayside cusp (near noon and 80 magnetic latitude). Most of the data we show are for the geomagnetic index K_p index in the range 3− to 3+ (displayed as '$K_p = 3$' in the figure annotations) because it is moderate or middle level activity. We also concentrate on the equinox season because it represents half the data set and because it is midway between summer and winter.

In Fig. 4, we show two separate groupings of the Joule heating rate data according to the IMF sector: the 'away' (IMF $B_y < 0$) and the 'toward' (IMF $B_x < 0$) IMF sectors. We have made this separation to look for the effect of the IMF structure upon the Joule heating rates. Some effect might be expected, since the IMF tends to pull ionospheric plasma convection from the noon meridian toward the morning (in the northern hemisphere during IMF away sectors—IMF $B_x < 0$ and IMF $B_y > 0$, on average) or toward afternoon (in the northern hemisphere IMF toward sectors—IMF $B_y > 0$ and IMF $B_x < 0$, on average). However, Fig. 4 shows little difference in

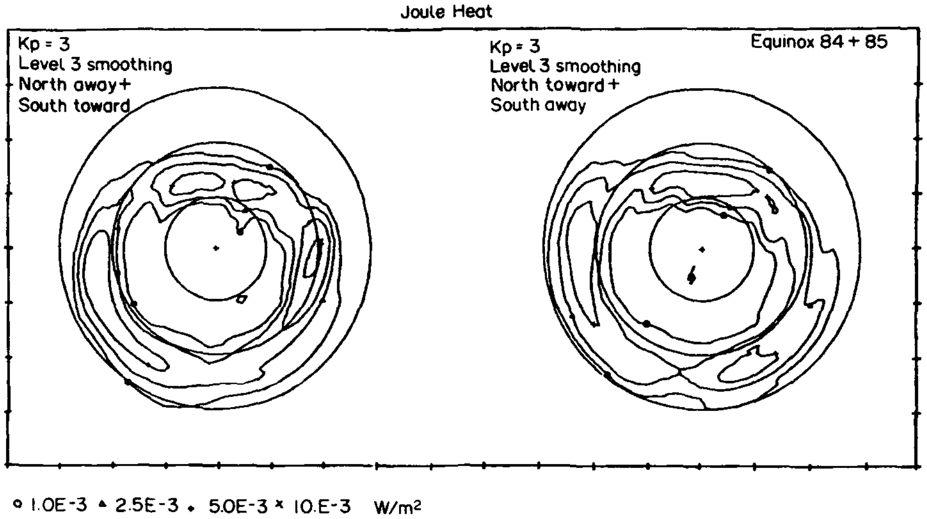

Fig. 4. Contour plot of average height-integrated Joule heating rate (W m^{-2}) determined from all DMSP/F7 data obtained during equinox for a moderate level of geomagnetic activity, $K_p = 3-$ to $3+$. The smoothing algorithm has been applied to the data three times before being displayed. The contour levels are from 1.0×10^{-3} to 1.0×10^{-2} W m^{-2}. The geomagnetic pole is marked with a cross and the geomagnetic latitudes of 80, 70 and 60° are shown; (a) plot annotated 'North Toward + South Away' represents equinox data from the northern hemisphere during times when the magnetic field within an interplanetary structure is pointed toward the Sun (IMF $B_y > 0$) combined with data from the southern hemisphere for IMF away sectors (IMF $B_y < 0$) (see the text for the explanation of why these data sets are joined); (b) plot annotated 'North Away + South Toward' represents equinox data from the northern hemisphere obtained during IMF away sectors (IMF $B_y < 0$) combined with data from the southern hemisphere obtained during IMF toward sectors (IMF $B_y > 0$). On average, IMF $B_z < 0$ when IMF $B_y > 0$, and IMF $B_z > 0$ when IMF $B_y < 0$.

the total Joule heat energy input pattern for the two sectors. There is a slight shift in local time of the pattern as the regions of rapid convection shift in response to the different magnetic stresses between the solar wind and magnetosphere for the positive and negative B_y. The shift in the maximum heating in the post-midnight sector is overemphasized by the filling and smoothing algorithm. Similar small changes in the Joule heating pattern with IMF sector changes are found for all other seasons and levels of geomagnetic activity.

In Fig. 5, a comparison of the Joule heating pattern for $K_p = 1$ and $K_p = 6$ demonstrates the variation in the pattern of Joule heating with increasing geomagnetic activity. As expected the total Joule heating and the maximum Joule heating rate increase and the equatorward edge of the heating zone expands equatorward as geomagnetic activity increases. The regions with the highest heating rates are within regions of downward field-aligned current where the particle-induced increase in conductivity is minimal. The region of maximum Joule heating in the auroral zone for the $K_p = 6$ map is more spread out than is generally true of any single high-active period, because this mapping level contains a wide variety of very high, very dynamic energy flow into the auroral zone. There is an anomalous region in the $K_p = 1$ map in the afternoon sector at sub-auroral latitudes (magnetic latitude ~62–67°, magnetic local time ~16–19 h). This region appears in maps for $K_p = 0$ and 1, but vanishes for higher levels of geomagnetic activity. This anomalous region is an artefact of our baseline fitting procedure yielding an incomplete fit for satellite tracks which pass obliquely through the auroral zone without reaching the polar cap.

In Fig. 6, we show the Joule heating rates obtained at the two extremes in season. In the summer season, the heating rate near the dayside cusp is enhanced and the heating rate in the auroral zone (especially the evening auroral zone) is depressed compared with that during the equinoxes and in the winter season. In the winter season, the heating rate near the dayside cusp is depressed and the heating rate in the auroral zone is enhanced.

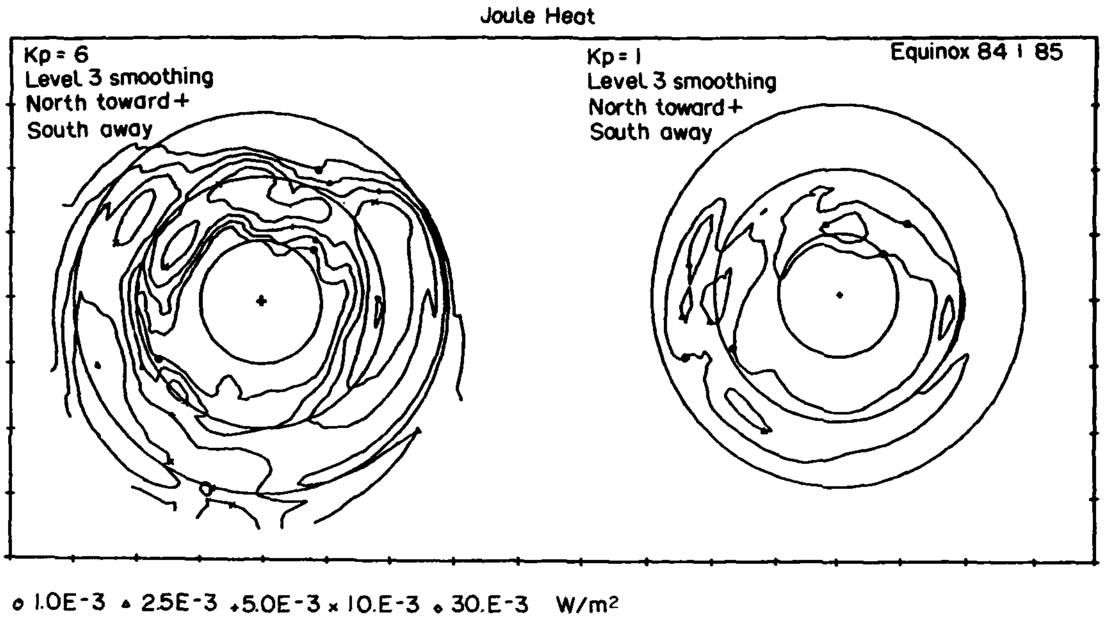

Fig. 5. Contour plot of average Joule heating rate in the same format as Fig. 4; (a) plot annotated '$K_p = 6$' represents data obtained during extremely disturbed geomagnetic times when $K_p = 6-$ to 9; (b) plot annotated '$K_p = 1$' represents data obtained during geomagnetically quiet times when $K_p = 1-$ to $1+$.

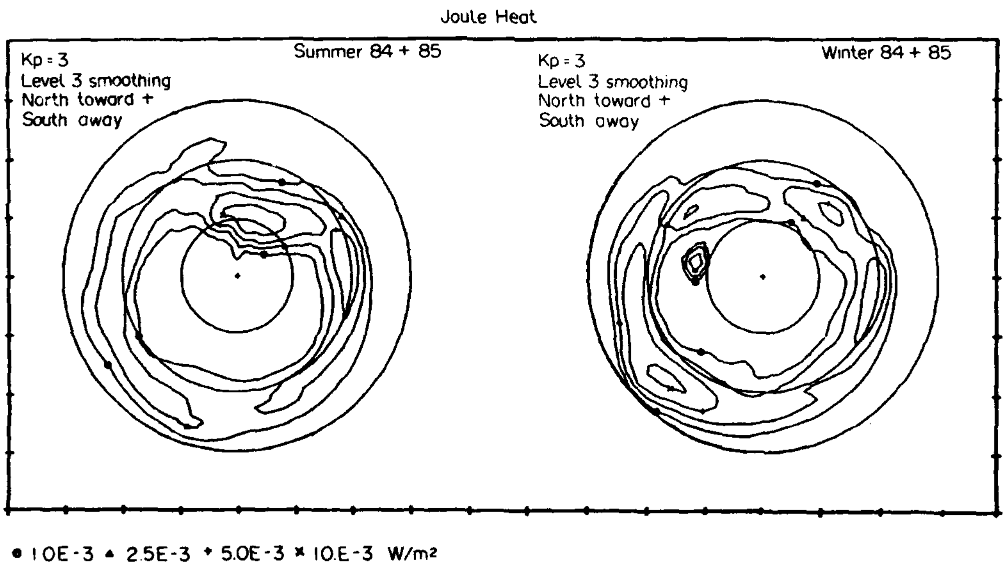

Fig. 6. Contour plot of average Joule heating rate in the same format as Fig. 4 for a moderate level of geomagnetic activity and data from the northern hemisphere for IMF toward sectors (IMF $B_y > 0$) and from the southern hemisphere for IMF away sectors (IMF $B_y < 0$); (a) Joule heating rate during summer months—May, June and July in the northern hemisphere and November, December and January in the southern hemisphere; (b) Joule heating rate during winter months.

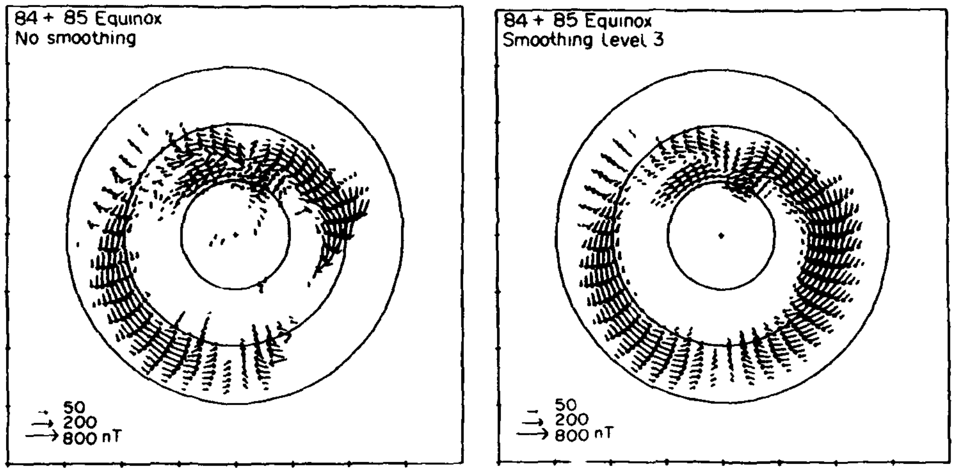

Kp = 3 North toward + south away
(a)

Kp = 3 North toward + south away
(b)

Fig. 7. Vector plot of average ΔB determined from all DMSP/F7 data obtained during 1984 and 1985 during equinox for a moderate level of geomagnetic activity, $K_p = 3-$ to $3+$. The geomagnetic pole is marked with a cross and the geomagnetic latitudes of 80, 70 and 60° are shown. Magnetic noon is at the top of the plot; 0600 h is at the right. Vectors in the southern hemisphere have been rotated 180° in order to match the vectors in the northern hemisphere. All data were obtained on days when the average IMF was in a toward sector (IMF $B_y > 0$, $B_z < 0$) when northern hemisphere data were obtained in an away sector (IMF $B_y > 0$, $B_z < 0$) when southern hemisphere data were obtained. (a) Plot of average vectors only for bins with data and without smoothing data with adjacent bins. (b) Plot of average vectors after filling in data by interpolation in bins without data and applying the smoothing algorithm three times.

4.2. *Average magnetic deflections*

In Fig. 7a, we display an example of the average magnetic deflection vectors without any smoothing or adding of vectors in regions not observed. In Fig. 7b, we display the same data after filling bins without data and after three iterations of the smoothing algorithm. The smoothing process has a small effect on the magnetic deflections in the later morning and early evening sectors where the currents are well ordered and there is a wealth of data. The smoothing process makes the pattern near the dayside cusp and cleft more orderly than the unsmoothed average deflections, but it does not change the basic character of the pattern. The pattern of deflections near the Harang discontinuity is not quite what would be expected from previous studies. Other investigators have reported a zone between approximately 2000 and 2400 h where convection (Hall current) is westward (eastward) on the poleward edge of the auroral zone and eastward (westward) on the equatorward edge. This is also observed as three zones of field-aligned current such as shown by Iijima and Potemra (1976). This pattern is not in the smoothed data because it does not exist in unsmoothed data. Also, the expected 'overlay' in the region of the Harang discontinuity is missing from most of our data set. Examination of individual satellite passes indicates many passes where the third current sheet on the poleward edge is missing or appears to be thin (1° or 2° in latitudinal width). It is possible that the third current sheet is not as thin as it appears. The thin portion of the current sheet is a region where deflection changes rapidly with latitude and is co-located with the poleward edge of precipitating auroral electrons. There is often a region poleward of the thin current sheet where the deflection is slowly changing with latitude and there is only 'polar rain' type precipitation. This region has been removed by our baseline fitting procedure, but it might be part of a downward field-aligned current carried by upward-flowing, cold electrons.

In Figs 8–10, we present the average magnetic deflection vector for the same conditions as in Figs 4–6. The center of each vector is placed at the center of the magnetic latitude/magnetic local time bin used to calculate the vector. The size of each vector represents the size of the average deflection for that bin. A blank region indicates either no data or an average deflection whose magnitude is less than 15 nT. Since we are averaging deflection vectors and Joule heating separately, regions where the average vector is close to

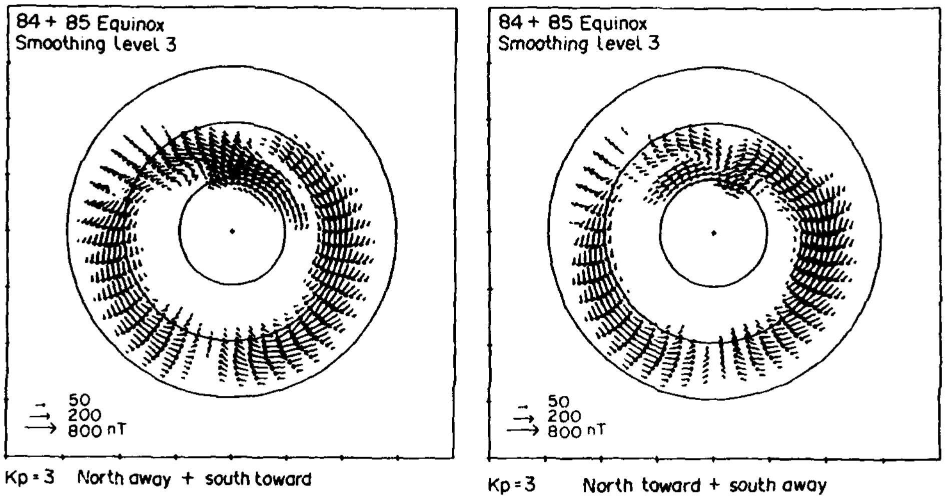

(a) (b)

Fig. 8. Vector plot of average ΔB in the same format as Fig. 7. All data obtained when K_p = 3− to 3+. (a) Equinox data from the southern hemisphere for IMF away sectors and from the northern hemisphere for IMF toward sectors. (b) Equinox data from the southern hemisphere for IMF toward sectors (IMF $B_y > 0$) and from the northern hemisphere for IMF away sectors (IMF $B_y < 0$).

zero will not have low values of average Joule heat if the variance is high.

The magnetic deflection vectors would be exactly proportional to the ionospheric plasma convection vectors after rotating each vector 180° if the ionospheric conductivity were uniform across the high-latitude region. Although the average high-latitude conductivity is not uniform, in general it does vary slowly as a function of latitude and local time, and thus the average magnetic deflection vectors are

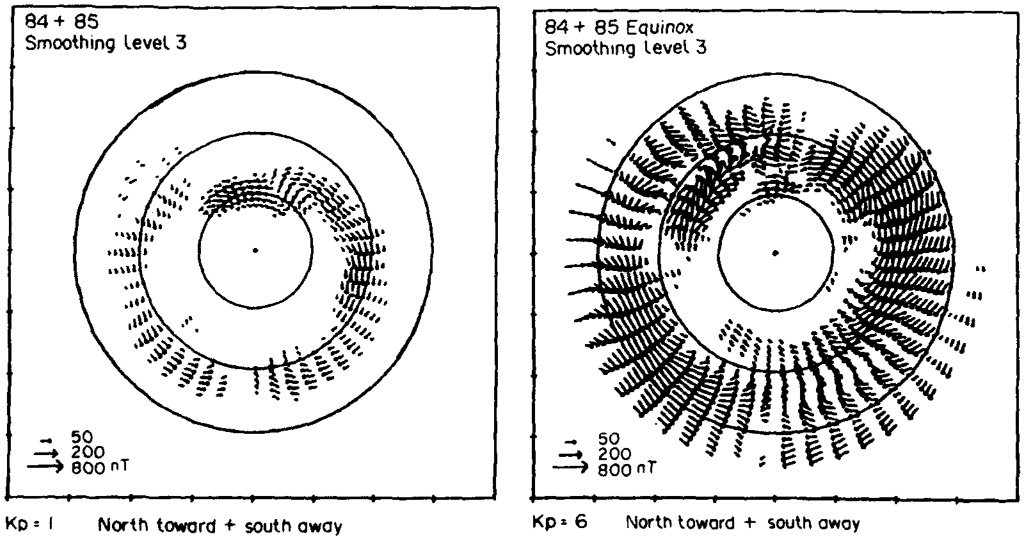

(a) (b)

Fig. 9. Vector plot of average ΔB in the same format as Fig. 7. All data obtained during the equinox seasons. (a) Data obtained during very low geomagnetic activity, K_p = 1− to 1+. (b) Data obtained during very high geomagnetic activity, K_p = 6− to 9.

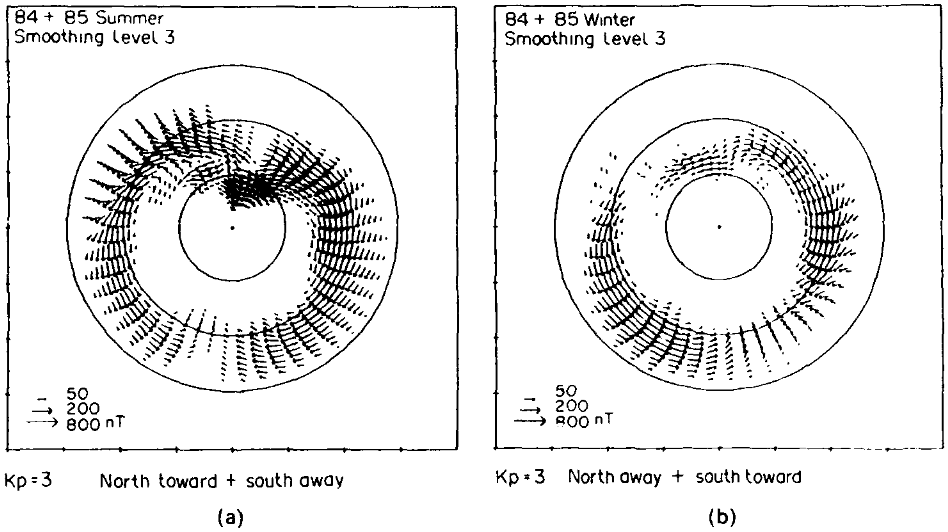

Fig. 10. Vector plot of average ΔB in the same format as Fig. 7. All data obtained during moderate geomagnetic activity, K_p = 3− to 3+. (a) Data obtained during the summer seasons. (b) Data obtained during the winter seasons.

roughly proportional to the average ionospheric plasma convection parameters. Because of the method we have used to find the baseline for the magnetic deflections, most of the magnetic deflections poleward of the auroral oval are zero. Based upon a comparison with patterns of the average electric field [e.g. HEPPNER and MAYNARD (1987)], we expect in the polar cap a nearly uniform set of magnetic deflection vectors, with magnitudes of a few tens of nT pointing sunward (anti-sunward plasma convection).

The magnetic deflections shown in Figs 8–10 clearly show the basic elements of the high-latitude, field-aligned current system first described by IIJIMA and POTEMRA (1976). In the morning and afternoon/evening auroral regions we find the anti-sunward convection region bounded by the pair of field-aligned region 1/region 2 currents: near noon we find the currents associated with the dayside cusp; and near midnight we find the reversal of currents and convection velocity and the Harang discontinuity. With the vast quantity of data used in this data set, we are able to create a much more detailed and quantified pattern of the high-latitude field-aligned current than has been previously available.

In Fig. 8, we show the effect of the change in IMF B_x component upon the average magnetic deflections. This is the same as showing the effect of the IMF B_y component. As expected from previous surveys of field-aligned currents, ionospheric currents and plasma convection, the most dramatic change is in the region of the ionospheric projection of the dayside cusp and cleft. When the IMF $B_x < 0$ and average IMF $B_y > 0$ (Fig. 8a), the ionospheric currents in the northern hemisphere polar cap are pulled to the morning side, and when the IMF $B_x > 0$ and average IMF $B_y < 0$ (Fig. 8b), they are pulled to the afternoon/evening side. The other notable change in the pattern with the change in the IMF is the shift in the Harang discontinuity from the 2315 h MLT meridian to the 2400 h MLT meridian in the northern hemisphere as the IMF changes from 'away' to 'toward'. This shift has not been commented upon as much as the shift in the noon pattern.

Figure 8 also shows that the average morning and afternoon/evening electrojets meet and turn poleward between 1100 and 1130 h MLT instead of at 1200 h as the IIJIMA and POTEMRA (1976) pattern showed. Most of this departure from the noon meridian can be accounted for by the 5°, or 20 min of local time, aberration angle of a radially outward solar wind due to the orbital motion of the Earth.

In Fig. 9, we show the effect of the change in the geomagnetic activity level upon the magnetic deflections. As shown in Fig. 9a, the currents associated with the dayside cusp decrease much less than the auroral currents as geomagnetic activity decreases. Also, the anomalous sub-auroral deflections in the afternoon sector which are discussed above are shown in Fig. 9a. As geomagnetic activity increases, the magnetic deflections and ionospheric currents in the aur-

oral zones increase significantly and the equatorward edge of the auroral currents and deflections moves equatorward. For the $K_p = 6$ level of binning, the non-zero deflections in the night sector extend equatorward of our lowest latitude bin, 55–56 . The poleward edge of the auroral currents and deflections changes only slightly with changing geomagnetic activity. The latitude of the dayside cusp/cleft deflections moves a few degrees equatorward with the change in activity.

In Fig. 10, we show the effect of the change from the summer season (with maximum solar-produced conductivity) to the winter season (with minimum conductivity) upon the magnetic deflections. As expected, there is a general decrease in the magnetic deflection and the resulting ionospheric currents as the solar-produced conductivity decrease. The decrease is less in the evening auroral zone than in the dayside auroral zone and dayside cusp/cleft region. The location of the cusp/cleft region also moves a few degrees equatorward as the polar region tilts away from the Sun. This change in cusp location with season has been previously reported by BURCH (1972) and by NEWELL and MENG (1989). The MLT meridian of the Harang discontinuity changes significantly with season from near 2300 h for summer to something in the range of 0100–0300 h for winter. The uncertainty of the winter locations is due to sparseness of data in that sector.

5. DISCUSSION

The validity of our Joule heat results are dependent upon the validity of the assumptions that we have made in estimating ionospheric currents and conductivity from our particle precipitation and magnetic field data. A study of Joule heating made by the incoherent radar station at Sondre Stromfjord, Greenland, independent of any DMSP data but simultaneous with some DMSP passes (WATERMANN and DE LA BEAUJARDIERE, 1990), indicates that our method is valid. The Joule heating derived from the two techniques are approximately equivalent. The radar measurements of the EUV component of the ionospheric conductivity indicate that our estimate of the EUV component tends to be too high. This comes from our use of the 10 7-cm radio flux as an indicator of the solar EUV flux. BARTH *et al.* (1990) have shown that the monthly averaged 10.7-cm radio flux is a good indicator of the Lyman alpha flux for moderate to high solar activity, but overestimated the Lyman alpha flux for the same period of low solar activity as our data set. If the Lyman alpha flux tracks the total EUV flux, then we have made a systematic error that would raise our estimates of Joule heat by 10–50%.

The magnitude and distribution of the height-integrated Joule heating rates in this study are comparable with those obtained by other investigators. The study of Joule heat made by FOSTER *et al.* (1983) using Atmospheric Explorer C ion drift and precipitating particle data near the minimum in the solar cycle is similar to our study. It was also a global survey for all seasons and geomagnetic activity levels. Due to the smaller data set, they sorted the AE-C data into much larger bins. They also found that the Joule heating was approximately co-located with the auroral oval and the dayside cusp. They found a local maximum near the dayside cusp, but they could not resolve the summer/winter asymmetry that we have found. Also, they could not clearly resolve the local maxima in Joule heating around the auroral oval. They did find that the results were more meaningful when Joule heat was calculated from simultaneous values of conductivity and electric field ($\langle Q \rangle = \langle \Sigma_P \cdot E^2 \rangle$) than from average values of conductivity and electric field ($\langle Q \rangle = \langle \Sigma_P \rangle \langle E^2 \rangle$). They also found that there was not a meaningful difference between the patterns for the spring and fall seasons. Overall, their maximum Joule heating rate was 3–6 mW/m^2 for low geomagnetic activity ($K_p = 0$–3) and was >8 mW/m^2 for high geomagnetic activity. We obtained slightly higher maximum heating rates because of our smaller bin size.

The study of HEELIS and COLEY (1988) is similar to that of FOSTER *et al.* (1983) in that they used ion drift data to determine the electric field driving the ionospheric currents. Using the simultaneous DE-2 ion temperature data, they determined the local Joule heating in the *F*-layer between 350 and 550 km altitude averaged over all seasons, all levels of geomagnetic activity and all IMF conditions. The distribution of the *F*-layer local Joule heat shows a poorly defined, high-latitude oval. There is a maximum in the local heating near 80 and 10–12 h MLT. When the ion drift data were combined with a model ionospheric conductivity, a clearly defined oval of height-integrated Joule heating appeared, but there was no maximum near the noon meridian. There were maxima of ~ 13 mW m^{-2} near 70 and 01 and 05 h. This pair of maxima is 30–50% larger than we obtained and showed in Fig. 4. Since the DE-2 data were obtained during the maximum in the solar cycle when the solar contribution to the conductivity was higher, we would expect from the model of KAN and SUN (1985) (see below) that the DE-2 heating would be higher than ours in the noon sector and lower than ours in the auroral zone. We have no explanation for the apparent contradiction between our results and the DE-2 results. We do feel that further study of the Joule

heating at the maximum in the solar cycle is needed in order to make a comparison with the results at solar minimum.

The studies by KAMIDE *et al.* (1986) and AHN *et al.* (1989a,b) are similar to ours in that they determined the ionospheric currents and the ionospheric conductivity simultaneously. Their studies differ from our study and the Foster study in that their studies were for particular times instead of being for all times. Both studies showed maxima in the Joule heating near 05 and 16 h in the vicinity of the auroral zone which are comparable with our results. Their maximum heating rates tended to be higher than ours by approximately 50% because they had not averaged their measurements over time and area. Both studies failed to show a significant region of heating near the dayside cusp/cleft. Since we find a prominent magnetic deflection in the noon sector for most satellite passes, we believe that these studies missed this portion of the Joule heating.

Joule heating rates have previously been computed from models of ionospheric parameters. RICH and MAYNARD (1989) used the patterns of the convection electric field of HEPPNER and MAYNARD (1987) together with the conductivity patterns of HARDY *et al.* (1987) to calculate patterns of Joule heat deposition. The Joule heat pattern in Fig. 4 for 'North Toward + South Away' should be comparable with the Joule heat for the Heppner–Maynard–Rich (HMR) model DE (IMF $B_y < 0$) and the 'North Away + South Toward' Joule heat pattern should be comparable with the Joule heat pattern for the HMR model BC (IMF $B_y > 0$). The magnitude of the Joule heating rates reported here is very similar to those calculated for the HMR models. The major difference is that the maximum heating for the dayside cusp moved significantly away from noon for the HMR models instead of being near the noon meridian as reported here. EVANS *et al.* (1987) made a calculation of Joule heat similar to the calculation of RICH and MAYNARD (1989) except for using the electric field model of FOSTER *et al.* (1986) based on data from the Millstone Hill radar and using the particle data from TIROS/NOAA. Their estimates of Joule heat in the auroral zones were similar to the other results mentioned herein, but their calculations missed the Joule heating in the dayside cusp region, since the Millstone radar could not see that far poleward.

KAN *et al.* (1988) used a simple, time-dependent model of the ionospheric response to a substorm. We cannot compare our results directly with Kan's model results or the results of any dynamic model due to the statistical nature of our results. Our results for $K_p = 1$ or 2 should be similar to the state of the auroral ionosphere used by a dynamic model at the time before the substorm, and our results for $K_p = 4$ or 5 should be similar to the state of a dynamic model after integrating over all time of the substorm expansion phase.

The change in the Joule heating as a function of season is an interesting feature of our patterns. Joule heat energy deposition would also be independent of season if it were co-located with the regions of maximum particle-produced ionization where $\Sigma_P(e\ ) \geqslant \Sigma_P(v)$. However, Joule heating tends to be a maximum in regions of downward field-aligned current where particle-produced ionization is important but does not dominate. Thus Joule heat tends to be deposited in high-latitude regions which have higher conductivity in the summer than in the winter. KAN and SUN (1985) have considered how the ionosphere would respond to different types of voltage generators in the magnetosphere. If the generator is a constant voltage generator, then the current and the Joule heat (I_P^2/Σ_P) flowing into the ionosphere would decrease with decreasing conductivity. If the generator is a constant current generator, then the current would be unchanged and the Joule heat input would increase as conductivity decreased. KAN and SUN (1985) indicated that a constant voltage generator must exist on open field lines in the magnetosphere and that a constant current generator must exist on closed field lines. From our results shown in Fig. 6, we conclude that the dayside cusp/cleft currents are driven by a generator on open field lines and that the auroral zone currents are driven by a generator on closed field lines.

The shift in the magnetic local time of the Harang discontinuity with changes in the level of geomagnetic activity and in the sign of the IMF B_y component has been discussed by previous investigators. For example, FOSTER *et al.* (1989) and SICA *et al.* (1989) have observed changes in the Harang discontinuity location due to changes in IMF B_y similar to our observations. On the other hand, HEPPNER and MAYNARD (1987) reported that their observations showed no evidence for a change in local time as a function of geomagnetic activity and only a change in magnetic latitude with changes in the IMF B_y component which they thought might be confused with a local time shift. Our observations are clearly in disagreement with Heppner and Maynard's conclusion. We have ruled out an error due to our statistical method by checking a few individual passes with similar conditions except for the IMF sector. The statistical maps of average magnetic deflections shown here are representative of our original data. Since the field lines in the Harang discontinuity region map to flux tubes well within the interior of the magnetosphere, we must conclude that

the IMF sector affects the basic structure of the magnetosphere and not just the boundary.

This survey provides a set of reference values for future observations and for computer models of the ionosphere, thermosphere and magnetosphere. The volume of data used provides a finer resolution of the spatial variations, seasonal variations and variations with geomagnetic activity than did previous surveys. While we have shown only part of the results here, the entire set of results is available to interested investigators.

6. CONCLUSIONS

As a result of surveying the magnetometer and precipitating electron data from DMSP/F7, we draw the following conclusions:

1. The IMF sector has little effect on the total Joule heat input to the high-latitude ionosphere and causes only a small rotation in local time of the pattern.

2. The dayside cusp as defined by the magnetic deflections and the Joule heating maximum moves slightly equatorward in winter; this 'dipole tilt effect' has been previously reported.

3. The magnitude of the field-aligned currents and Joule heat in the region of the dayside cusp decreases with decreasing conductivity. The source of the field-aligned currents into/out of the dayside cusp region is a constant voltage source, which implies that the source is on open field lines [KAN and SUN (1985)].

4. The magnitude of the field-aligned currents into/out of the evening sector is independent of season; the Joule heat is a maximum in winter and a minimum in summer. The source of the field-aligned currents into/out of the evening sector is a constant source, which implies the source is on closed field lines [KAN and SUN (1985)].

5. The location of the Harang discontinuity as defined by the magnetic deflections changes in local time as a function of season. It moves toward the early morning in winter and mid-evening in the summer.

6. The Harang discontinuity in the northern hemisphere as defined by the magnetic deflections moves to earlier local times for IMF B_y away sectors (IMF $B_y > 0$) than found during IMF B_y toward sectors (IMF $B_y < 0$).

Acknowledgement—Analysis of DMSP data is supported by the Air Force Office of Scientific Research under Task 2311G5.

REFERENCES

AHN B.-H., KROEHL H. W., KAMIDE Y. and GORNEY D. J. 1989b Estimate of ionospheric electrodynamic parameters using ionospheric conductance deduced from bremmstrahlung X-ray image data. *J. geophys. Res.* **94**, 2565.

AHN B.-H., KROEHL H. W., KAMIDE Y., GORNEY, D. J., AKASOFU S.-I. and KAN J. R. 1989a The auroral energy deposition of the polar ionosphere during substorms. *Planet. Space Sci.* **37**, 239.

BARON M. J. and WAND R. H. 1983 *F* region ion temperature enhancements resulting from Joule heating. *J. geophys. Res.* **88**, 4114.

BARTH C. A., TOBISKA W. K., ROTTMAN G. J. and WHITE O. R. 1990 Comparison of 10.7 cm radio flux with SME solar Lyman Alpha flux. *Geophys. Res. Lett.* **17**, 571.

BUCHERT S. and LA HOZ C. 1988 Extreme ionospheric effects in the presence of high electric fields. *Nature* **333**, 438.

BURCH J. L. 1972 Precipitation of low-energy electrons at high latitudes: effects of interplanetary magnetic field and dipole tilt angle. *J. geophys. Res.* **77**, 6696.

EMERY B. A., ROBLE R. G., RIDLEY E. C., KILLEEN T. L., REES M. H., WINNINGHAM J. D., CARIGNAN G. R., HAYES P. B., HEELIS R. A., HANSON W. B., SPENCER N. W., BRACE L. H. and SUGIURA M. 1985 Thermospheric and ionospheric structure of the southern hemisphere polar cap on 21 October 1981 as determined from Dynamics Explorer 2 satellite data. *J. geophys. Res.* **90**, 6553.

EVANS D. S., FULLER-ROWELL T. J., MAEDA S. and FOSTER J. 1987 Specification of the heat input to the thermosphere from magnetospheric processes using TIROS/NOAA auroral particle observations. *Astrodynamics* **64**, 1649.

FOSTER J. C., FULLER-ROWELL T. and EVANS D. S. 1989 Quantitative patterns of large-scale field-aligned current in the auroral ionosphere. *J. geophys. Res.* **94**, 2555.

FOSTER J. C., HOLT J. M., MUSGROVE R. G. and EVANS D. S. 1986 Ionospheric convection associated with discrete levels of particle precipitation. *Geophys. Res. Lett.* **13**, 656.

FOSTER J. C., ST-MAURICE J.-P. and ABREU V. J. 1983 Joule heating at high latitudes. *J. geophys. Res.* **88**, 4885.

FULLER-ROWELL T. and EVANS D. S. 1987 Height-integrated Pedersen and Hall conductivity patterns inferred from the NOAA-TIROS satellite data. *J. geophys. Res.* **92,** 7606.

GUSSENHOVEN M. S., HARDY D. A. and CAROVILLANO R. L. 1985 Average electron precipitation in the polar cusps, cleft and cap. In *The Polar Cusp*, HOLTET J. A. and EGELAND A. (eds). D. Reidel, Dordrecht.

HARDY D. A., GUSSENHOVEN M. S. and BRAUTIGAM D. 1989 A statistical model of auroral ion precipitation. *J. geophys. Res.* **94,** 370.

HARDY D. A., GUSSENHOVEN M. S. and HOLEMAN E. 1985 A statistical model of auroral electron precipitation. *J. geophys. Res.* **90,** 4229.

HARDY D. A., GUSSENHOVEN M. S., RAISTRICK R. and MCNEIL W. J. 1987 Statistical and functional representations of the pattern of auroral energy flux, number flux and conductivity. *J. geophys. Res.* **92,** 12275.

HEDIN A. E. 1983 A revised thermospheric model based on mass spectrometer and incoherent scatter data: MSIS-83. *J. geophys. Res.* **88,** 10170.

HEDIN A. E. 1987 MSIS-86 thermospheric model. *J. geophys. Res.* **92,** 4649.

HEDIN A. E., REBER A., NEWTON G. P., SPENCER N. W., BRINTON H. C., MAYR H. G. and POTTER W. E. 1977b A global thermospheric model based on mass spectrometer and incoherent scatter data, MSIS 1, N_2 density and temperature. *J. geophys. Res.* **82,** 2148.

HEDIN A. E., SALAH J. E., EVANS J. V., REBER C. A., NEWTON G. P., SPENCER N. W., KAYSER D. C., ALCAYDE D., BAUER P., COGGER L. and MCCLURE J. P. 1977a A global thermospheric model based on mass spectrometer and incoherent scatter data, MSIS 1, N_2 density and temperature. *J. geophys. Res.* **82,** 2139.

HEELIS R. A. and COLEY W. R. 1988 Global and local Joule heating effects seen by DE 2. *J. geophys. Res.* **93,** 7551.

HEPPNER J. P. and MAYNARD N. C. 1987 Empirical high-latitude electric field models. *J. geophys. Res.* **92,** 4467.

IIJIMA T. and POTEMRA T. A. 1976 The amplitude distribution of field-aligned currents at northern high latitudes observed by Triad. *J. geophys. Res.* **81,** 2165.

KAMIDE Y. and BAUMJOHANN W. 1985 Estimate of electric fields and currents from international magnetospheric study magnetometer data for the CDAW 6 intervals: implications for substorm dynamics. *J. geophys. Res.* **90,** 1305.

KAMIDE Y., CRAVEN J. D., FRANK L. A., AHN B.-H. and AKASOFU S.-I. 1986 Modeling substorm currents systems using conductivity distributions inferred from DE auroral images. *J. geophys. Res.* **91,** 11235.

KAMIDE Y., ISHIHARA Y., KILLEEN T. L., CRAVEN J. D., FRANK L. A. and HEELIS R. A. 1989 Combining electric field and auroral observations from DE1 and 2 with ground magnetometer records to estimate ionospheric electromagnetic quantities. *J. geophys. Res.* **94,** 6723.

KAN J. R. and SUN W. 1985 Simulation of the westward traveling surge and *Pi*2 pulsations during substorms. *J. geophys. Res.* **90,** 10911.

KAN J. R., ZHU L. and AKASOFU S.-I. 1988 A theory of substorms: onset and subsidence. *J. geophys. Res.* **93,** 5624.

KILLEEN T. L., HAYS P. B., CARIGNAN G. R., HEELIS R. A., HANSON W. B., SPENCER N. W. and BRACE L. H. 1984 Ion neutral coupling in the high latitude *F*-region evaluation of ion heating terms from Dynamics Explorer 2. *J. geophys. Res.* **89,** 7495.

KILLEEN T. L. and ROBLE R. G. 1984 An analysis of the high-latitude thermospheric wind pattern calculated by a thermospheric general circulation model. I—Momentum forcing. *J. geophys. Res.* **89,** 7509.

KILLEEN T. L. and ROBLE R. G. 1986 An analysis of the high-latitude thermospheric wind pattern calculated by a thermospheric general circulation model. I—Neutral parcel transport. *J. geophys. Res.* **91,** 11291.

MARCOS F. A. 1989 Accuracy of atmospheric drag models at low satellite altitudes. *Adv. Space Res.* **10,** (in press).

NEWELL P. T. and MENG C. I. 1989 Dipole tilt angle effects on the latitude of the cusp and cleft/low-latitude boundary layer. *J. geophys. Res.* **94,** 6949.

RICH F. J., GUSSENHOVEN M. S. and GREENSPAN M. E. 1987 Observations by DMSP satellites of the energy flow into the high latitude ionosphere. *Ann. Geophysicae* **5,** 527.

RICH F. J., HARDY D. A. and GUSSENHOVEN M. S. 1985 Enhanced ionosphere-magnetosphere data from the DMSP satellites. *EOS, Trans. Amer. Geophys. Union* **66**, 513.

RICH F. J. and MAYNARD N. C. 1989 Consequences of using simple analytical functions for the high-latitude convection electric field. *J. geophys. Res.* **94**, 3687.

SICA R. J., HERNANDEZ G., EMERY B. A., ROBLE R. G., SMITH R. W. and REES M. H. 1989 The control of auroral zone dynamics and thermodynamics by the interplanetary magnetic field dawn–dusk (*Y*) component. *J. geophys. Res.* **94**, 11921.

VICKREY J. F., VONDRAK R. R. and MATTHEWS S. J. 1982 Energy deposition by precipitating particles and Joule dissipation in the auroral ionosphere. *J. geophys. Res.* **87**, 5184.

WATERMANN J. and BEAUJARDIERE O. DE LA 1990 Joule heating investigations using the Sondrestrom radar and DMSP satellites. Technical report GL-TR-90-0172, Geophysics Laboratory Hanscom AFB, Bedford, Massachusetts, U.S.A.